

# Integrated-Holographic Coarse-Wavelength-Division Multiplexers Patterned by DUV Photolithography

Christoph M. Greiner, *Member, IEEE*, Dmitri Iazikov, *Associate Member, IEEE*,  
and Thomas W. Mossberg, *Member, IEEE*

**Abstract**—We demonstrate monolithically integrated four and eight-channel coarse-wavelength-division multiplexers with low insertion loss (IL) and wide flat-top passbands based on integrated-holographic filters. Like thin-film filters (TFFs), integrated-holographic filters function via a multipath interference and thus offer flexible passband control without the IL penalty that passband shaping typically incurs in single-mode angularly dispersive devices. Unlike TFF-based multiplexers, the multiplexers described here are based on the silica-on-silicon planar lightwave circuit platform rather than discrete optics and thus uniquely provide powerful TFF-like filtering function in fully integrated format. The multiplexer performance demonstrated is superior to the integrated solutions demonstrated to date, and competitive with discrete TFF-based devices.

## I. INTRODUCTION

MULTIPLEXING is a critical function in all areas of the wavelength-division multiplexing (WDM) network, and the quest for optimal solutions appropriate to the specific deployment areas is an ongoing one. Today's multiplexing approaches can be loosely divided in two categories: integrated (e.g., arrayed waveguide grating (AWG) based) and discrete (e.g., thin-film filter (TFF) based). Both technologies have their strengths and weaknesses.

Widely used integrated solutions are primarily based on reflective or transmissive gratings, e.g., AWGs [1]–[3] or echelle gratings [4], [5]. Due to their inherent capability to parallel-process signals, these devices are attractive for situations involving high channel counts. Furthermore, the integrated format of the planar lightwave circuit platform that is typically used provides a natural pathway to ultimately low fabrication cost.

Physically, AWG and echelle gratings function on the basis of angular dispersion which makes them well suited to route many signal channels with Gaussian-like passbands into separate output channels. However, as angularly dispersive devices, they have a fundamental limitation when the channels of complex passband (spanning a range of output directions) need to be mapped into single-mode outputs. While angularly dispersive filters can be configured to deliver tailored, e.g., flat top, passbands into single-mode outputs, doing so requires an insertion-loss (IL) penalty, which becomes more severe as the number of grating resolution bandwidths coupled to

the output increases [6], [7]. Recently, double grating devices interconnected with a waveguide array have been shown to more flexibly route tailored passbands into single-mode outputs [8], [9]. In these devices, the second grating realigns the selected angularly dispersed signals into a common output direction. The addition of the second grating provides substantially more passband flexibility, but on the other hand, it increases the device complexity and size and thus ultimately increases cost and limits wafer yield.

Angular dispersion is not the only spectral filtering mechanism available. TFFs operate by a different principle, i.e., multipath interference. Passbands are defined through the interaction of unidirectional light with a series of dielectric interfaces. Quite general passbands can be achieved and routed to single-mode outputs without a fundamental IL penalty, but TFF-based multiplexers typically consist of hand-assembled systems of daisy-chained discrete filters. Package size and fabrication complexity of such devices increases with the channel number favoring implementation with relatively low channel counts. Furthermore, the package footprint is often constrained by the approximately 2-in minimum bending diameter required for long-term mechanical reliability of the interconnection fiber.

In this paper, we describe a new multiplexing approach that combines the strengths of spectral filtering based on multipath interference with the planar lightwave circuit platform, thus delivering the passband flexibility that is normally reserved to discrete thin-film devices and doing so in a fully integrated format. The multiplexers reported here are based on integrated-holographic two-dimensional (2-D) (volume) gratings. Like thin-film devices, integrated-holographic filters function via multipath interference and thus offer flexible passband control without IL penalty [10], [11]. In fact, integrated-holographic devices may functionally be thought of as integrated TFFs. The reflective interfaces of the integrated-holographic filter, lithographically etched trenches, are curved so that they provide focusing of signals between input and output ports as well as providing arbitrary passband tailoring. The devices described here are applicable to any WDM standard, and are enabled by the high-resolution patterning newly available through advances in deep ultraviolet (DUV) photolithography [10], [11]. Recognition of the general potential of DUV photolithography for integrated photonics fabrication is presently emerging in the community [11]–[13]. Multiplexing and general filtering based on integrated-holographic devices is a material-agnostic approach and can be combined with other device functionalities. Here, we report on the design and fabrication of high-performance single-mode integrated coarse WDM (CWDM)

Manuscript received June 9, 2006; revised November 9, 2006.

The authors are with LightSmyth Technologies, Inc., Eugene, OR 97042 USA (e-mail: cgreiner@lightsmyth.com; diazikov@lightsmyth.com; twmoss@lightsmyth.com).

Digital Object Identifier 10.1109/JLT.2006.888163

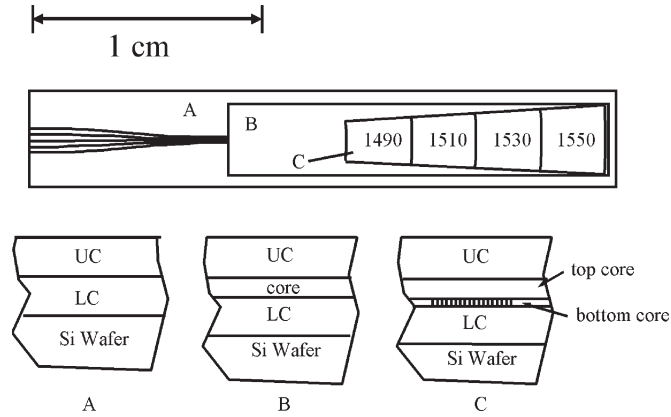


Fig. 1. Schematic top view of four-channel CWDM multiplexer chip with cross-sectional views of (A) nonguiding, (B) slab, and (C) filter regions.

multiplexers [14]—a function very difficult to realize with prior integrated filtering technologies. The performance realized is competitive with traditional thin-film CWDM devices.

Note that recently investigated photonic crystal filters based on one-dimensional (1-D) waveguides [15], [16] can also provide TFF or Bragg grating like spectral design flexibility in an integrated format. A strongpoint of the present integrated-holographic technology is that the 2-D gratings separate the filtered reflected signals from the input without requiring additional elements such as circulators or couplers that are necessary in the former 1-D approach.

## II. DEVICE LAYOUT

Fig. 1 shows schematics of a four-channel coarse-wavelength-division multiplexer based on integrated-holographic filters. The uppermost figure is a top view that looks down on the silica-on-silicon die comprising the multiplexer and illustrates the device operation. Horizontal lines on the left of the die represent channel waveguides that are used for signal input and output. For demultiplexing, input signals are in-coupled via the central common channel waveguide from whose endpoint they expand into a slab waveguide region (region B). To the right of the slab region are four stacked  $\sim 2.7$ -mm-long integrated-holographic filters whose resonance wavelengths increase with distance from the input port in increments of 20 nm (region C). Each of the four filters focuses signals emerging from the common channel and within its respective reflection passband to one of the outlying four channels. The focusing action is reciprocal, enabling multiplexing and demultiplexing function. The overall die dimensions are approximately  $4 \times 26$  mm<sup>2</sup>.

The lower three schematics in Fig. 1 are partial device cross sections corresponding to locations A, B, and C on the device die. Region A is nonguiding, region B is the prefilter slab waveguide, and region C contains the integrated volume gratings. In the cross-sectional views, the upper and lower cladding layers are, respectively, doped silica and thermal oxide. Both cladding layers have a thickness of  $\sim 14$   $\mu$ m and a refractive index of  $\sim 1.45$ . In region B, the core is a single layer of approximately 2.3- $\mu$ m thickness. In region C, the 2.3- $\mu$ m core comprises two layers. Here, the upper core layer has a refractive

index about 0.7% above the cladding index, while the lower core layer has a +3% index differential with respect to the latter. Both core sublayers consist of doped silica glass. In all regions, only a single vertical spatial mode is supported. The diffractive contours comprising the volume holographic grating individually image a portion of the input signal to the output channel. In the present instance, a unity-conjugate ratio imaging is employed, but the contours can be configured to provide optimal wavefront matching between ports of essentially arbitrary nature. The diffractive contours of a given CWDM channel filter are circular and concentric about the midpoint between the ends of the common input and the specific output waveguides. There are about 5400 diffractive contours in each filter section. The higher index core layer serves the important function of shifting the signal mode to better overlap the etched diffractive contours, and therefore increase the reflective coupling. Scanning electron micrographs of typical grating cross-sectional profiles similar to the devices fabricated here can be found in [17].

At the present, we have chosen to implement the CWDM device in the silica-on-silicon planar lightwave circuit platform with relatively low index contrast due to its proven low-loss character [18] and the need for efficient fiber-to-waveguide coupling, as is demonstrated below. The integrated-holographic technology is generally material agnostic, and the implementation in higher index contrast materials, such as silicon-on-insulator, can lead to device footprints that can in principle be made as small as those of, e.g., photonic crystals [19].

## III. FABRICATION

The 2-D Bragg gratings comprising the multiplexer and located in region C were realized in the lower subcore layer by the use of a DUV optical scanner with  $4\times$  reduction ratio from a laser-written chromium-on-quartz reticle and subsequent reactive ion etching. The scanner provides the necessary resolution, of order  $\lambda/4$  in the material, i.e., 250 nm, to realize the 2-D gratings. Following the chemical vapor deposition of the upper core layer, the common and output channel waveguides were defined via i-line photolithography and etch followed by final cladding deposition.

## IV. MEASUREMENTS

### A. Spectral Transfer Function

Fig. 2 shows the reflection spectrum of each of the four integrated filters as measured at its respective output channel. The IL shown includes a 1.3-dB fiber-to-die coupling loss determined in separate measurements, which is consistent with the refractive indices and channel waveguide dimensions. On-chip loss of the first channel (about 1.6-dB IL) is thus only about 0.3 dB. By the fourth channel, the IL has increased to approximately 2.4 dB. It is believed that the on-chip loss comes from a combination of out-of-plane scattering introduced by the apodization method and from avoidable film inhomogeneities that interfere with focusing into the output channels. Both effects accumulate with total propagation length and hence channel number. The passband flatness is found to be better

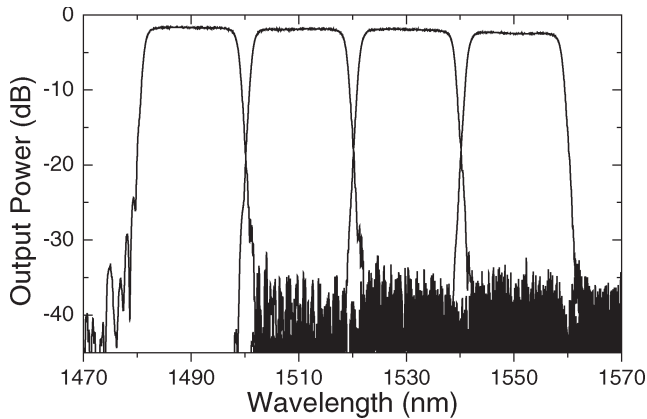


Fig. 2. Reflection passbands for the four channels comprising the multiplexer/demultiplexer. Output power levels shown include all losses including fiber to die.

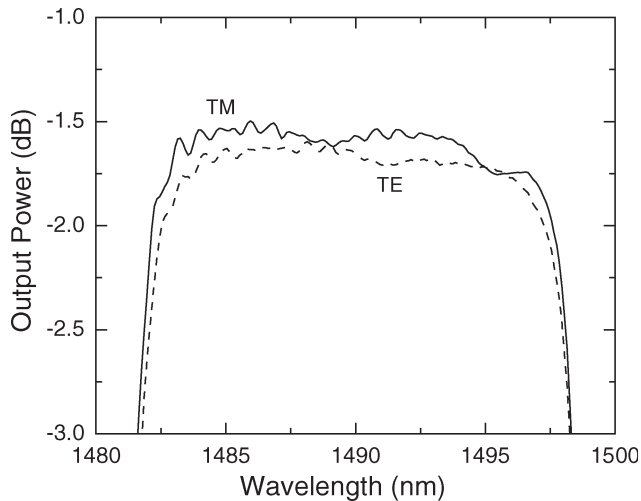


Fig. 3. Blowup of 1490-nm multiplexer passband explicitly showing the minimal polarization dependence.

than 0.3 dB. Isolation between adjacent channels is better than 34 dB. Part of the observed channel crosstalk is attributed to scattering from other gratings adjacent to the CWDM filter (not shown in Fig. 1) that would not be part of a dedicated production run. Increases in the spacing of the output channel waveguides (as they enter the slab region) are also expected to reduce the crosstalk.

Fig. 3 shows an enlarged view of the first channel's passband with both polarizations shown. The polarization-dependent loss (PDL) is less than 0.2 dB across the 13-nm CWDM standard passband. The same value is found for the remaining three channels that are not shown here. We believe that the low PDL comes from a combination of three factors: 1) All reflections are at near normal incidence; 2) the maximal index contrast employed is only a few percent; and 3) the filters operate in the high reflection limit. The last factor is important since the polarization dependent reflectivity is suppressed in the high reflectivity limit. A polarization-dependent wavelength shift of 85 pm, entirely negligible compared to the width of the passband, was observed.

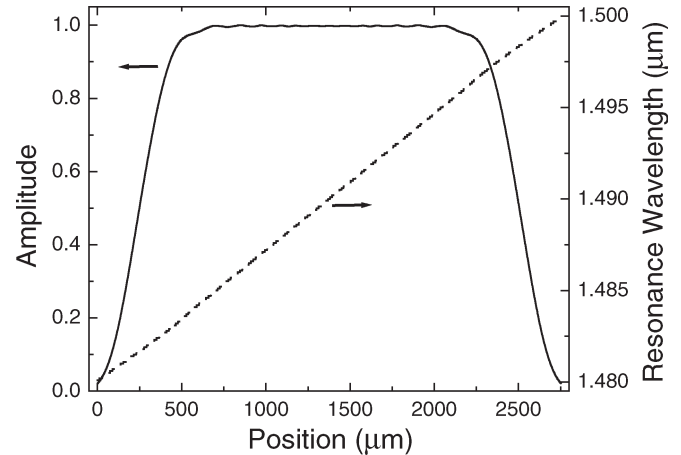


Fig. 4. Local reflective amplitude (solid line) and wavelength (dashed line) of first multiplexer channel as a function of position. The distance from the channel waveguide manifold increases with position.

### B. Device Apodization

Coarse wavelength division multiplexing requires flat-top passbands with low IL and wide passband widths with rapid filter falloff to yield the required levels of adjacent channel isolation. These features are clearly demonstrated in Fig. 2 and are difficult to achieve at acceptable IL levels with competing single-mode compatible integrated filters [8], [9].

In the present integrated filters, wide passbands are achieved by chirping the average spacing of the diffractive contours within the gratings. Varying the local grating period in this fashion yields a position-dependent resonance wavelength, illustrated as a dashed line in Fig. 4 for the first filter of the four-channel multiplexer. Elimination of passband ripple, typical of chirped gratings, and rapid filter falloff in the wings of the filter passband, is accomplished through apodizing the reflective amplitude of the filters. The amplitude apodization function employed is shown as a solid line in Fig. 4.

To physically realize the apodization function shown, a correlated-line scheme [17] was used. In correlated-line apodization, the local reflective amplitude of small sets of grating elements is interferometrically controlled by appropriately spacing their constituent elements to yield the desired set amplitude. In Fig. 5, we show the specific contour spacings versus the position within the filter that were used to achieve the amplitude apodization of Fig. 4. As illustrated in Fig. 5, low reflective amplitude values in the filter passband wings were realized by spacing the contours of the multiline sets more closely than the nominal  $\lambda/2$ -spacing. (The large spacing values plotted at the ends of the filter correspond to the spacings between multiline sets). Amplitude values above 0.98 are treated as unity, so that in the central grating region (corresponding to the main passband), the spacing is a simple chirp (see inset). The advantage of the correlated-line apodization method is that it is fully consistent with standard binary (single depth) contour etching.

To demonstrate the impact of filter apodization more directly, an unapodized integrated-holographic filter was constructed for comparison. The general layout of the unapodized device was similar to that of an individual channel filter of Fig. 1, with

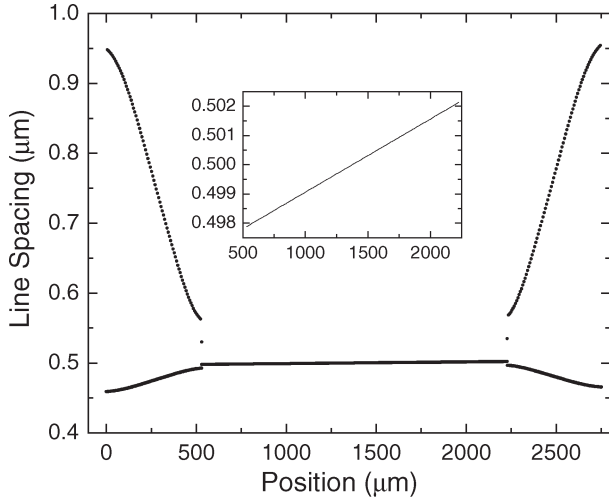


Fig. 5. Spacing between adjacent diffractive contours comprising the 1490-nm integrated-holographic filter. Rapid variations at the beginning and end of the filter indicate contour displacements necessary to interferometrically apodize the local reflective amplitude. Inset shows the central chirped region with an increased vertical resolution.

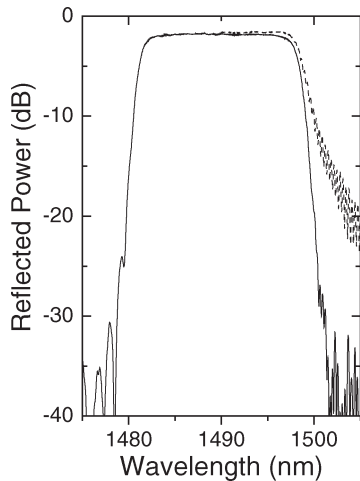


Fig. 6. Comparison of passband falloff for apodized (solid line) and unapodized (dashed line) filters.

the exception that the grating is slightly shorter (2.3 mm). In the unapodized filter, the contour spacing follows a linear chirp with position-independent reflection amplitude. Fig. 6 compares the filter response of the apodized multiplexer channel filter (solid line) with the relevant portion of the unapodized device's spectrum shown as a dashed line. As expected, the passband of the unapodized filter falls off significantly more slowly in the wings.

### C. Dispersion Properties

Fig. 7 shows the measured group delay versus the wavelength within the passband of the 1550-nm channel as measured with an HP 86037B chromatic dispersion test system. Dashed lines indicate the 13-nm wide CWDM passband standard. Within this passband, the average chromatic dispersion, given by the slope of the group delay versus the wavelength plot, is 1.4 ps/nm. Consequently, at a bit rate of 10 Gb/s, the device dispersion of about 1.1 ps is essentially negligible. The dispersion prop-

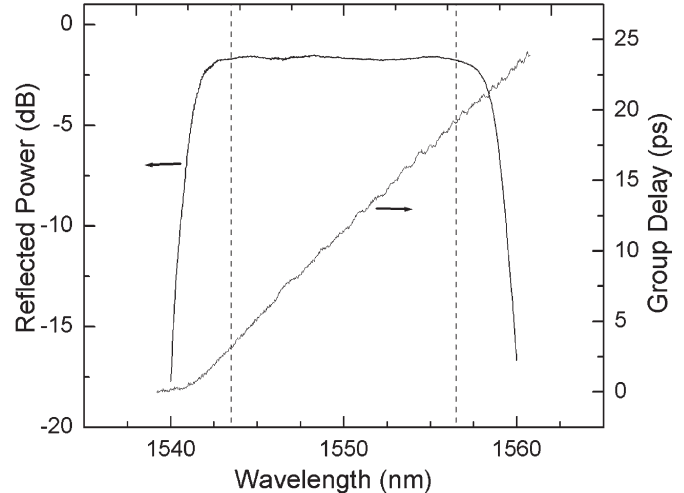


Fig. 7. Group delay versus wavelength for 1550-nm channel filter. Dashed lines denote standard 13-nm passband. Dispersion properties for other channels are similar.

erties observed in Fig. 7 are dominated by the grating's period chirp. The observed behavior is similar for the other channels. It is interesting to note that chirped integrated-holographic filters, such as the ones presented here, provide the capability to simultaneously demultiplex and dispersion compensate incoming signals.

### D. Passive Device Athermalization

The multiplexers' channel filter passbands were found to shift with temperature at a rate of  $\sim 10$  pm/ $^{\circ}$ C. As can be seen in the example of Fig. 3, the passbands were designed to substantially exceed the 13-nm CWDM standard. The excess width serves as a guardband that is sufficiently wide to make the device passively athermal over approximately 100  $^{\circ}$ C.

### E. Eight-Channel CWDM Multiplexer

For deployment as multiplexers, where minimizing the channel crosstalk is less critical than in demultiplexing, the filter apodization can be less crucial. We have fabricated an eight-channel CWDM multiplexer based on the unapodized channel filters. The layout of the device is generally similar to that shown in Fig. 1, with the exception that the gratings are slightly shorter, ranging from 2.3 mm for the first (1470 nm) channel to 2.5 mm for the last (1610 nm). Grating lengths are increasing with wavelength, as the number of lines for each channel was kept constant at 4572. Filter periods are linearly chirped to achieve the required passband width. The overall die size for the eight-channel unit is only  $4.5 \times 33$  mm<sup>2</sup>.

In Fig. 8, we show the measured eight-channel multiplexer spectral transfer function. The bluest six multiplexer channels were characterized by the use of a tunable laser. The 1590- and 1610-nm channel filters were measured using a light emitting diode-based broadband source and an optical spectral analyzer. For these two channels, only spectral portions above the measurement noise floor are shown. Less spectral detail is observed due to the coarser,  $\sim 0.3$ -nm resolution. Falloff characteristics

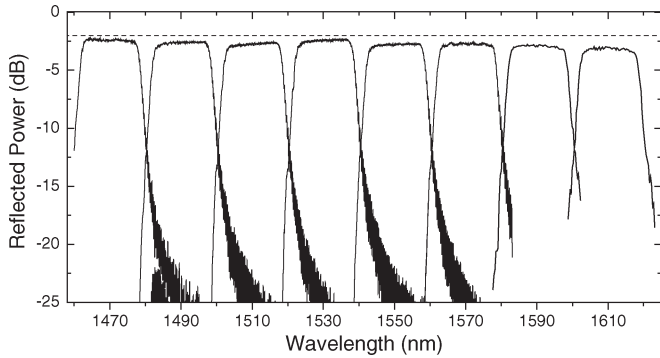


Fig. 8. Reflection passbands for the eight-channel multiplexer. Output power levels shown include all losses including fiber to die.

are expected to be similar to the first six channels. The dashed line in Fig. 8 corresponds to a 2-dB IL.

The IL of the first channel of the multiplexer is about 2.3 dB; the final channel of the apodized device has an IL about 0.8-dB higher. IL variations are attributed to film inhomogeneities that can be improved through a refinement of fabrication techniques and alterations in internal design to reduce sensitivity to film variations.

## V. CONCLUSION

To summarize, monolithically integrated single-mode compatible multiplexers, based on integrated-holographic filters and providing uniquely wide, flat, and low-IL passbands, have been demonstrated and found to be superior to all existing integrated and competitive with existing TFF-based alternatives. Integrated-holographic filters function via the same principle as thin-film devices but do so in a fully integrated rather than discrete environment and incorporate signal routing function as well. Lithographically scribed integrated-holographic filtering elements will provide an important building-block element for future photonic integration providing a unique low IL passband control. Stamping or injection-molding-based production [20], [21] from photolithographically fabricated masters will provide a pathway to high-volume low-cost devices for access and data centric applications.

## ACKNOWLEDGMENT

The authors would like to thank D. Le, K. McGreer, and T. Ticknor of NeoPhotonics Corporation for providing the group-delay measurement described here.

## REFERENCES

- [1] M. K. Smit, "New focusing and dispersive planar component based on an optical phased array," *Electron. Lett.*, vol. 24, no. 7, pp. 385–386, Mar. 1988.
- [2] H. Takahashi, S. Suzuki, K. Kato, and I. Nishi, "Arrayed waveguide grating for wavelength division multi/demultiplexer with nanometer resolution," *Electron. Lett.*, vol. 26, no. 2, pp. 87–88, Jan. 1990.
- [3] C. Dragone, "An  $N \times N$  optical multiplexer using a planar arrangement of two star couplers," *IEEE Photon. Technol. Lett.*, vol. 3, no. 9, pp. 812–815, Sep. 1991.
- [4] J. He, B. Lamontagne, A. Delage, L. Erickson, M. Davies, and E. S. Koteles, "Monolithic integrated wavelength demultiplexer based on a waveguide rowland circle grating in InGaAsP/InP," *J. Lightw. Technol.*, vol. 16, no. 4, pp. 631–638, Apr. 1998.

- [5] V. I. Tolstikhin, A. Densmore, K. Pimenov, Y. Logvin, F. Wu, S. Laframboise, and S. Grabtchak, "Monolithically integrated optical channel monitor for DWDM transmission systems," *J. Lightw. Technol.*, vol. 22, no. 1, pp. 146–153, Jan. 2004.
- [6] W. R. Babbitt and T. W. Mossberg, "Optical waveform processing and routing with structured surface gratings," *Opt. Commun.*, vol. 148, no. 1–3, pp. 23–26, Mar. 1998.
- [7] K. Okamoto and H. Yamada, "Arrayed-waveguide grating multiplexer with flat spectral response," *Opt. Lett.*, vol. 20, no. 1, pp. 43–45, Jan. 1995.
- [8] C. R. Doerr, M. Cappuzzo, L. Gomez, E. Chen, A. Wong-Foy, C. Ho, J. Lam, and K. McGreer, "Planar lightwave circuit eight-channel CWDM multiplexer with < 3.9-dB insertion loss," *J. Lightw. Technol.*, vol. 23, no. 1, pp. 62–65, Jan. 2005.
- [9] C. R. Doerr, R. Pafchek, and L. W. Stulz, "Integrated band demultiplexer using waveguide grating routers," *IEEE Photon. Technol. Lett.*, vol. 15, no. 8, pp. 1088–1090, Aug. 2003.
- [10] T. W. Mossberg, "Planar holographic optical processing devices," *Opt. Lett.*, vol. 26, no. 7, pp. 414–416, Apr. 2001.
- [11] C. Greiner, D. Iazikov, and T. W. Mossberg, "Lithographically-fabricated planar holographic Bragg reflectors," *J. Lightw. Technol.*, vol. 22, no. 1, pp. 136–145, Jan. 2004.
- [12] W. Bogaerts, V. Wiaux, D. Taillaert, S. Beckx, B. Luyssaert, P. Bienstmann, and R. Baets, "Fabrication of photonic crystals in silicon-on-insulator using 248-nm deep UV photolithography," *J. Sel. Topics Quantum Electron.*, vol. 8, no. 4, pp. 928–934, Jul./Aug. 2002.
- [13] M. Settle, M. Salib, A. Michaeli, and T. F. Krauss, "Low loss silicon on insulator photonic crystal waveguides made by 193 nm optical lithography," *Opt. Express*, vol. 14, no. 6, pp. 2440–2445, Mar. 2006.
- [14] D. Iazikov, C. Greiner, and T. W. Mossberg, "Integrated holographic filters for flat-passband optical multiplexers," presented at the Optical Fiber Commun. Conf., Anaheim, CA, 2006, Paper PDP11.
- [15] A. S. Jugessur, P. Pottier, and R. M. De La Rue, "Engineering the filter response of photonic crystal microcavity filters," *Opt. Express*, vol. 12, no. 7, pp. 1304–1312, Apr. 2004.
- [16] M. Davanco, A. Xing, J. W. Raring, E. L. Hu, and D. J. Blumenthal, "Compact broadband photonic crystal filters with reduced back-reflections for monolithic InP-based photonic integrated circuits," *IEEE Photon. Technol. Lett.*, vol. 18, no. 10, pp. 1155–1157, May 2006.
- [17] T. W. Mossberg, C. Greiner, and D. Iazikov, "Interferometric amplitude apodization of integrated gratings," *Opt. Express*, vol. 13, no. 7, pp. 2419–2426, Apr. 2005.
- [18] R. Adar, M. R. Serbin, and V. Mizrah, "Less than 1 dB per meter propagation loss of silica waveguides measured using a ring resonator," *J. Lightw. Technol.*, vol. 12, no. 8, pp. 1369–1372, Aug. 1994.
- [19] C. Greiner, D. Iazikov, and T. W. Mossberg, "Fourier transform-limited performance of a lithographically-scribed planar holographic Bragg reflector," *IEEE Photon. Technol. Lett.*, vol. 16, no. 3, pp. 840–842, Mar. 2004.
- [20] D.-H. Kim, J.-G. Im, S.-S. Lee, S. W. Ahn, and K.-D. Lee, "Polymeric microring resonator using nanoimprint techniques based on a stamp incorporating a smoothing buffer layer," *IEEE Photon. Technol. Lett.*, vol. 17, no. 11, pp. 2352–2354, Nov. 2005.
- [21] J. Liu, Y.-L. Lam, Y.-C. Chan, Y. Zhou, B. S. Ooi, G. Tan, and J. Yao, "Embossed Bragg gratings based on organically modified silane waveguides in InP," *Appl. Opt.*, vol. 39, no. 27, pp. 4942–4945, Sep. 2000.

**Christoph M. Greiner** (M'02), photograph and biography not available at the time of publication.

**Dmitri Iazikov** (M'03–A'03), photograph and biography not available at the time of publication.

**Thomas W. Mossberg** (M'96), photograph and biography not available at the time of publication.